8-18-2022

Numerical Analysis of Offset Heatsinks

Alex Dutton
Washington University in St. Louis

Numerical Analysis of Offset Heatsinks

Alex Dutton

MEMS 5000 Independent Study

22 August 2022

"I hereby certify that the report herein is my original academic work, completed in accordance to the McKelvey School of Engineering and Undergraduate Student academic integrity policies, and submitted to fulfill the requirements of this assignment."

1 Abstract

As silicon production becomes cheaper, electronics use will become more widespread and diversified, such as through the use of 5G technologies, the internet of things, and the growth of enterprise computing through the cloud. As the demand for electronics grows, so too will the need for diverse thermal management technologies. Current thermal management methods range from passive elements such as heatsinks, to active two phase systems. Within the domain of heatsinks there exists many different manufacturing methods and geometries to meet a range of thermal challenges. Several manufacturing methods for heatsinks include: extruding, skiving, and bonding fins to base-plates. Each manufacturing method involves its own pros and cons; skived heatsinks have high thermal conductivity and can achieve high aspect ratio fins, however are not geometrically complex. Bonded or folded fin heatsinks can achieve various geometries and form factors due to the freedom from bonding of the fins, however the bond introduces additional thermal resistance to the heatsink. This research strives to study the impact of adding an offset to typical skived fin geometries on the friction factor and heat transfer from the heatsink. An analytical model of parallel fin heatsinks is developed and used to validate a 3D turbulent heat transfer simulation of parallel and offset fin heatsinks. A figure of merit (FOM) is used to simultaneously compare the friction factor and Nusselt number of the different heatsinks. A suite of simulations on various geometries of parallel fin and offset fin heatsinks is conducted, and they demonstrates that adding the offset results in an increase in the FOM of 30.3%. This demonstrates that an offset skived heatsink has better thermal performance without significantly increasing the pumping power required to cool the heatsink. This results in a heatsink that can cool higher thermal loads without increasing the energy consumed by the fans used to cool it.

2 Introduction

Heatsinks are a common method of dissipating the heat generated by electronic components. By using high conductivity materials with large surface areas, they are able to efficiently spread the heat away from the electronics and convect it into the air. One of the methods of creating aluminium or copper heatsinks is called skiving. Skived heatsinks are created by using a sharp blade to shave off thin parts of a monolithic work piece to create fins with high aspect ratios and fin densities. Currently available skived heatsinks come in two geometric variations, continuous fin and co-linear fin heatsinks. Both geometries are shown in fig. 1 and 2 below.

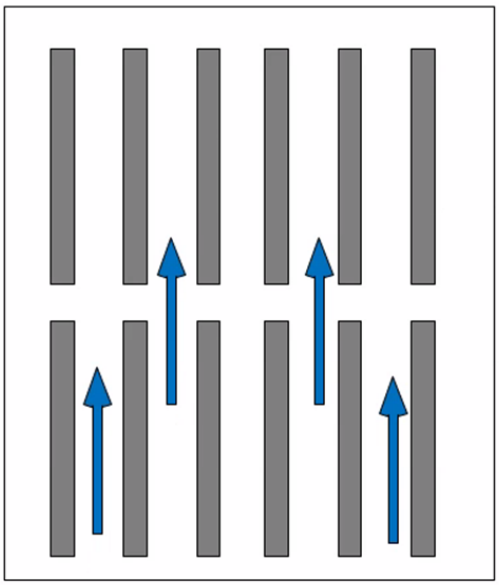

Figure 1: Image of Co-linear Fins

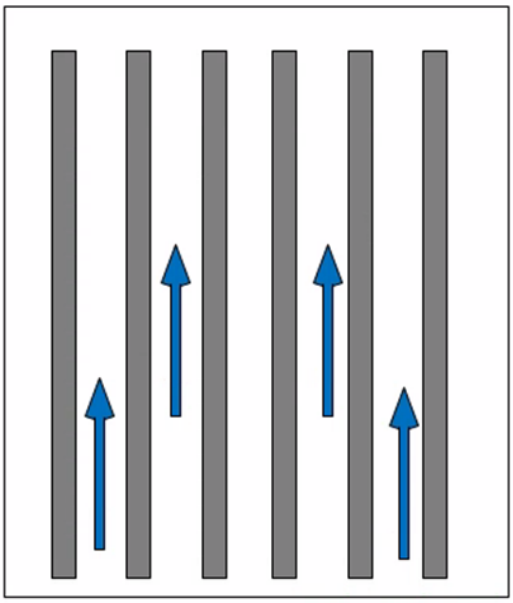

Figure 2: Image of Continuous Fins

This research seeks to add an additional geometric variation to skived heatsinks, an offset fin geometry. An example of the offset fin geometry is shown in fig. 3 below.

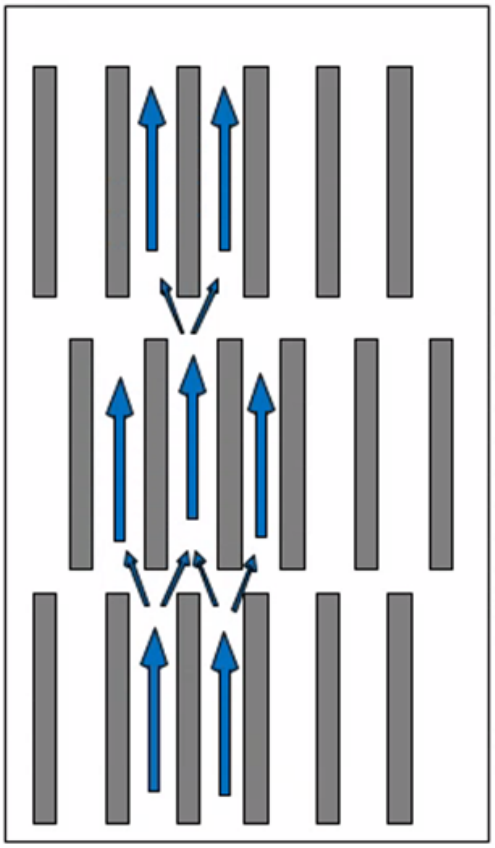

Figure 3: Image of an Offset Fin Heatsink

An initial design exploration into offset skived heatsinks was conducted by Dutton, Levy, and Luberda [1]. The initial investigation proposed a modification to a heat sink skiving blade that would result in manufacturing offset fins. It also conducted a cursory design of experiments (DOE) to investigate the impact of adding the offset. The results of this work indicated that further analysis needed to be conducted with higher fin densities, and with higher resolution within the boundary layer to more accurately capture the additional mixing caused by the offset. Additionally, Luberda further investigated the different parameters necessary to skive aluminium heatsinks [2]. The manufacturing exploration provided values on typical fin thicknesses, and manufacturable fin and row gaps that are used in this paper.

The analytical and numerical analysis present in this paper dive into the impact of the addition of the offset on the development on the hydraulic and thermal boundary layers between each of the pairs of fins.

3 Analysis

Two analysis methods are performed. First, an analytical method is developed to predict the heat transfer between two parallel plates, which is used to check the accuracy of the next analysis method, a 3D turbulent CFD simulation. The CFD model is then used to study the impact of adding an offset on the overall heat transfer of the solution.

3.1 Analytic Analysis

3.1.1 Developing Flow

Before studying the flow through the heatsink, a model studying the developing flow between parallel plates is created. This model seeks to find the most efficient channel length for the given fin thickness, fin height, and fin gap. The following section covers the solution to thermally and hydraulically developing flow for a rectangular channel [3].

The Nusselt and Reynolds number relationship for this problem is shown in eqn. 1.

$$Nu = \frac{\frac{3.66}{tanh(2.264*Gz_h^{-1/3}+1.7*Gz_h^{-2/3})} + 0.0449Gz_h tanh(Gz_h^{-1})}{tanh(2.432 * Pr^{1/6} * Gz_h^{-1/6})} \tag{1}$$

where Pr is the Prandtl number for the fluid, and Gz_h is the Graetz number and is shown in the equation below.

$$Gz_h = (D_h/x) * Re_{dh} * Pr \tag{2}$$

Re_{dh} is the Reynolds number. A modification is made to the traditional Nusselt number relationships, substituting the hydraulic diameter in for the traditional diameter when calculating the Reynolds number. The equation to calculate the hydraulic diameter D_h [m] is shown below [4].

$$D_h = \frac{4 * Area}{Perimeter} \tag{3}$$

The Reynolds number can then be calculated from the hydraulic diameter from eqn. 4

$$Re_{dh} = \frac{U * D_h}{\mu} \tag{4}$$

This assumption allows for the analysis of non-circular pipes using traditional pipe flow equations.

Typically the flow is assumed to be fully developed when $Gz_h^{-1} = 0.05$ [3]. For a fin with a height of 0.0254m, fin gap of 0.0036m, and air velocity of 10 m/s the development length is 0.7136m. This means that for the fin lengths under study, between 0.0085-0.032m, the flow will always be developing. This simplifies simplifies the analytical analysis in the next section, as the solution does not need to blend between a developing and developed flow solution.

The asymptotic behavior of the Nusselt Number along the length of the entrance region is shown in fig. 4 below.

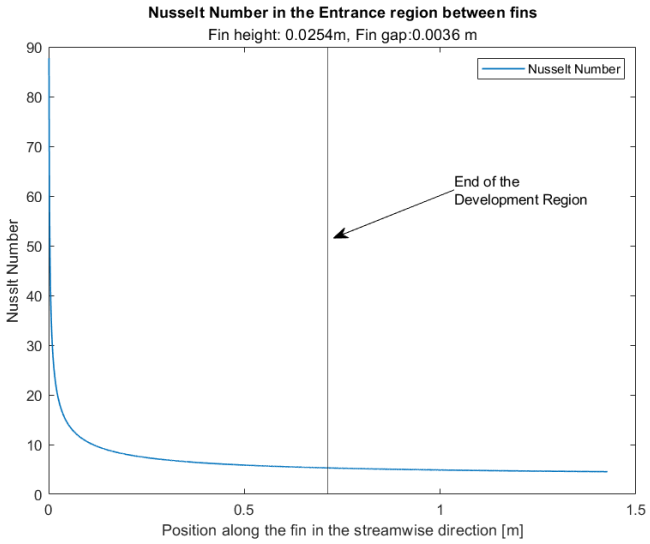

Figure 4: Graph of the Nusselt Number along the length of the fin

This behavior demonstrates that as the fin gets longer, the average heat transfer coefficient decreases. One common method of mitigating this effect is to disrupt the formation of the thermal and hydraulic boundary layer along the fin.

3.1.2 Heatsink Analytic Solution

After understanding the behavior of the Nusselt number in the developing region, an analytical solution for the flow between parallel fins is developed. The solution to flow between parallel fins proposed by Teertstra, Yovanavitch, and Culham [5], used here, accounts for the developing flow through the rectangular channels of a heatsink. Using a different Nusselt and Reynolds relationship for laminar developing flow through rectangular ducts, as well as traditional fin efficiency methods, a modified Nusselt number can be calculated. The system of equations used to calculate the heat transfer coefficient is shown below.

First the Reynolds number (Re_b) is calculated using the Fin Gap [m], fluid velocity U [m/s], and the fluid viscosity μ $[\frac{N*s}{m^2}]$.

$$Re_b = \frac{U * FinGap}{\mu} \tag{5}$$

Then the Channel Reynolds number (Re_b*) is calculated from the Reynolds number , fin gap and fin length.

$$Re_{b*} = \frac{Re_b * FinGap}{FinLength} \tag{6}$$

The average Nusselt number can then be calculated from eqn. 7.

$$Nu_{dev} = 0.664 * \sqrt{Re_{b*}} * Pr^{1/3} * (1 + (3.65/\sqrt{(Re_{b*})})) \tag{7}$$

Lastly, a fin efficiency modification is used to account for the conduction along the length of the fin, which creates a non-uniform temperature distribution along the fin height. The traditional fin efficiency equations are shown below in eqn. 8 and 9

$$m = sqrt(h * P/(k_{heatsink} * Area)) \tag{8}$$

$$\eta = tanh(m * Height)/(m * Height) \tag{9}$$

Where P is the perimeter of the fin, and η is the fin efficiency. The fin efficiency is used to calculate the final estimation for the Nusselt number $[Nu_{fineffect}]$, as shown below.

$$Nu_{fineffect} = eta * Nu_{dev}; \tag{10}$$

3.2 Simulation Setup

3.2.1 Simulation Geometry and Boundary Conditions

A parametric model of the heatsink is created in Ansys Design Modeler in order to speed up the simulation of several different geometries. The critical parametric dimensions and relationships are shown in fig. 5 below.

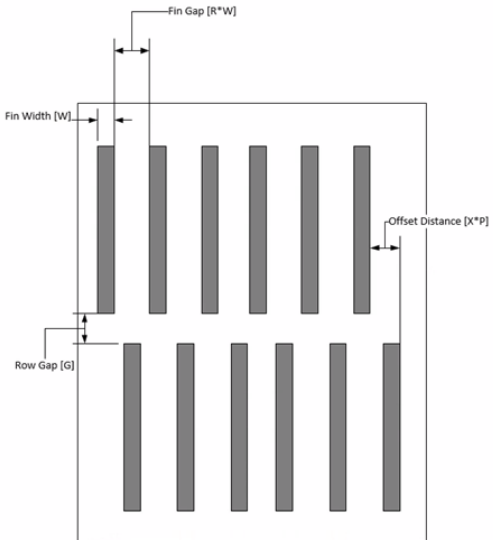

Figure 5: Geometric definitions of the fin geometries

All dimensions are in meters, with W as the fin width, and R as the Fin gap ratio, which is calculated from the fin width and fin gap as shown in eqn.

$$R = \frac{FinGap}{W} \tag{11}$$

Lastly, P is the fin pitch, which is defined as in the equation below

$$P = W * (1 + FinGap) \tag{12}$$

The offset distance can be calculated from X, the offset [dimensionless], and the fin pitch by eqn. 13 below.

$$OffsetDistance = X * P \tag{13}$$

Below is a table of the different parameter values under study. A sweep of the design space looking at different combinations of these parameters is conducted.

Fin Gap Ratio	Channel length	Row Gap	Offset
1.5	0.0085	0.002	0
1.8	0.125	0.001	0.5
2	0.03		

Figure 6: Table of the Design Parameters

3.2.2 Boundary Conditions

In order to account for the convection through the air, and the conduction from the heatsink, a conjugate heat transfer model is created. This involved separating the computational domain into 3 main sections, the heatsink base, Fins, and Fluid Domain. The different domains are shown in fig. 7 below.

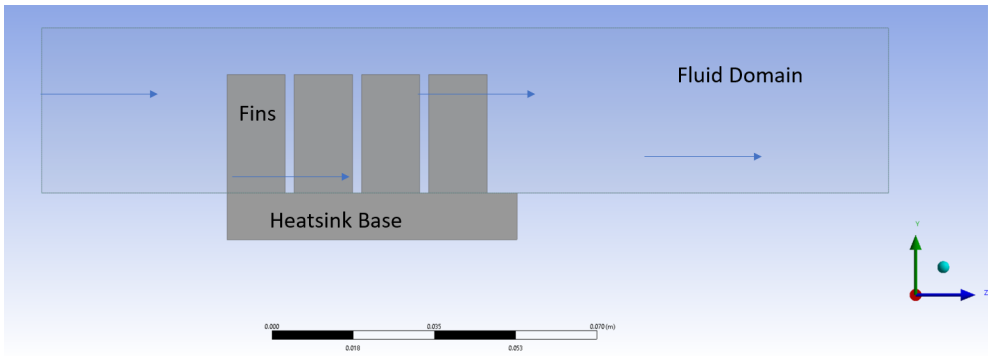

Figure 7: Image of the Solid and Fluid Domains of the Conjugate Heat Transfer Problem

The boundary conditions for the domain are shown in fig. 8 below.

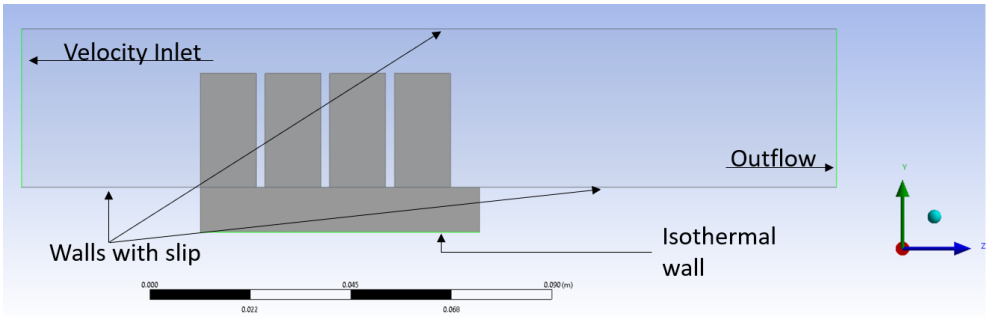

Figure 8: Boundary Condition Locations

The inlet velocity is 10 $\frac{m}{s}$, the inlet temperature is 300°K, and the temperature of the wall is 358°K, which is 85 ° C, a typical critical temperature for silicon microelectronics.

The last boundary conditions used are 2 periodic faces on the sides of the computational domain, as shown in fig. 9

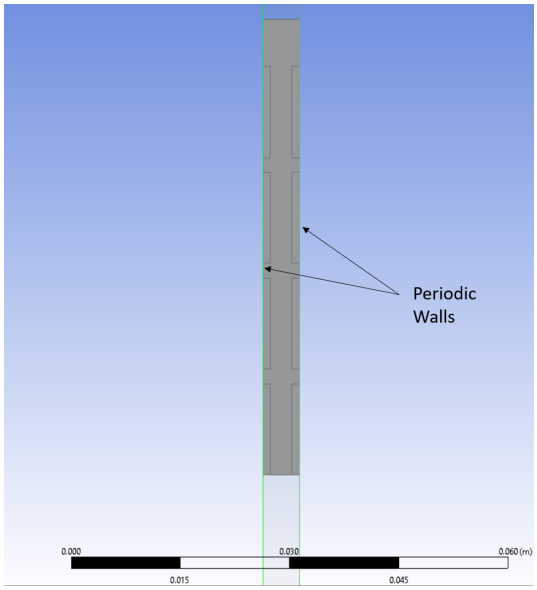

Figure 9: Image of the Periodic Boundaries

These periodic faces allow for the simulation of repeated rows of fins without the added computational complexity of simulating the additional fins. Therefore the solutions proposed from this analysis is only valid for the interior fins of a heatsink.

3.2.3 Mesh Sizing

Since the focus of this suite of simulations is to capture the additional mixing and turbulence introduced by the offset, it is critical to capture the entire boundary layer of the internal flow between both fins. In order to realize the viscous sublayer, a mesh of $y+ = 1$ is desired. $y+$ is a dimensionless measurement of the distance from the wall. A mesh with $y+ = 1$ has the first cell placed inside of the viscous sublayer, so the entire boundary layer is simulated. If the fluid

velocity, fin height, and fin gap are known,the physical distance from the wall, y [m], can be calculated as a function of $y+$ from the system of equations below. [6]

$$C_f = \frac{16}{Re_{dh}} \tag{14}$$

$$\tau_{wall} = 0.5 * C_f * \rho * U^2; \tag{15}$$

$$U_t = \sqrt{\tau_{wall}/\rho} \tag{16}$$

$$y = \frac{y_+ * \nu}{U_t} \tag{17}$$

where U is the fluid velocity $[\frac{m}{s}]$, μ is the dynamic viscosity $[\frac{N*s}{m^2}]$, Re_{dh} is the Reynolds number based off of the hydraulic diameter [unitless], C_f is the skin friction coefficient [unitless], ρ is the fluid density $[\frac{kg}{m^3}]$, τ_{wall} is the wall shear stress $[\frac{N}{m^2}]$, U_t is the wall friction velocity $[\frac{m}{s}]$, and ν is the kinematic viscosity $[\frac{m^2}{s}]$. The turbulenace model used for these simulations, the $k-\omega$ model, is valid throughout the near wall region, and by creating a mesh with a y+ of 1, there is no need for wall functions to model the buffer or viscous sublayer. [7] Ansys Fluent meshing was used to create a hexcore mesh of around 9 million cells for each geometry under study.

3.2.4 Governing Equations and Solution Methods

A conjugate heat transfer model was created in Ansys Fluent to account for both the conduction through the heatsink as well as the convection through the air. The governing equations used for these 3D steady state, coupled fluid/thermal simulations are the Reynolds Averaged Navier Stokes, or RANS Equations, and are shown below [8] [9].

$$\frac{\partial}{\partial x_i}(\rho U_i) = 0 \tag{18}$$

$$\frac{\partial}{\partial x_j}(\rho U_i U_j) = -\frac{\partial \rho}{\partial x_i} + \frac{\partial}{\partial x_j}[\mu(\frac{\partial U_i}{\partial x_j} + \frac{\partial U_j}{\partial x_i} - \frac{2}{3}\delta_{ij}\frac{\partial U_l}{\partial x_l})] + \frac{\partial}{\partial x_j}(-\rho\overline{U_i' U_j'}) \tag{19}$$

$$\nabla \cdot (\rho U(c_p T + U^2/2)) = \nabla \cdot (k_{eff}\nabla T + \tau_{eff} \cdot \vec{U}) \tag{20}$$

Where eqn. 18, 19, and eqn. 20 are the mass, momentum, and energy continuity equations respectively. U is the fluid velocity, k_{eff} is the effective fluid thermal conductivity, ρ is the fluid density, c_p is the specific heat of the fluid, and τ_{eff} is the effective fluid shear stress $[\frac{N}{m^2}]$. The SST $k-\omega$ turbulence model is used to calculate the Reynolds stress $-\rho\overline{U_i' U_j'}$ as well as the turbulent thermal conductivity and the effective shear stress. This provides closure to the RANS equations above.

For the solid domain, the governing conduction equation is given by the equation below [9]

$$0 = k_{solid}\nabla^2 T \tag{21}$$

4 Results

4.1 Analytical Results

The table below shows the results of the analytical solution for the flow between fins for a given fin configuration.

Inputs		Results	
Fin Height	0.0254	Average Nusselt Number	13.4665
Fin Length	0.0125	Average Heat Transfer Coefficient [W/(m^2*K)	105.12
Fin Gap [m	0.0036	Total Heat Transfer [W]	16.024
Number of Fins	4		

Figure 10: Table of results from the analytical methods

4.2 Numerical Results

Heatsink performance can be categorized by two different metrics: the heat transfer from the heatsink, and the impedance to flow. Generally these performance metrics are opposed to one another, with increases in overall heat transfer leading to greater impedances to the air flow. Increased airflow impedance leads to higher pumping powers, and an increase in flow bypass around the heatsink. The goal when designing the heatsink is to improve the overall heat transfer without significantly increasing the pumping power. In order to asses the different geometries on both metrics, a figure of merit is used, and is shown in eqn. 22. [10]

$$FOM = \frac{Nu/Nu_0}{(f/f_0)^{1/3}} \tag{22}$$

Several permutations on the parallel fin and offset geometry were simulated, and full results of the simulations can be found in fig. 20. Several key conclusions from the suite of simulations are shown in the following sections.

4.2.1 Parallel Fin Results

As discussed in section 3.1.1, the Nusselt number decreases with channel length. Therefore it is advantageous to disrupt the thermal and hydraulic boundary layer to get it to start to develop again. One method of disrupting the boundary layer is to introduce a gap into the channel walls. The distance between the rows of fins then becomes critical to how the boundary layer

is disrupted. The two graphs below in figures 11 and 12 analyze the impact of the gap distance on the skin friction coefficient and heat transfer respectively.

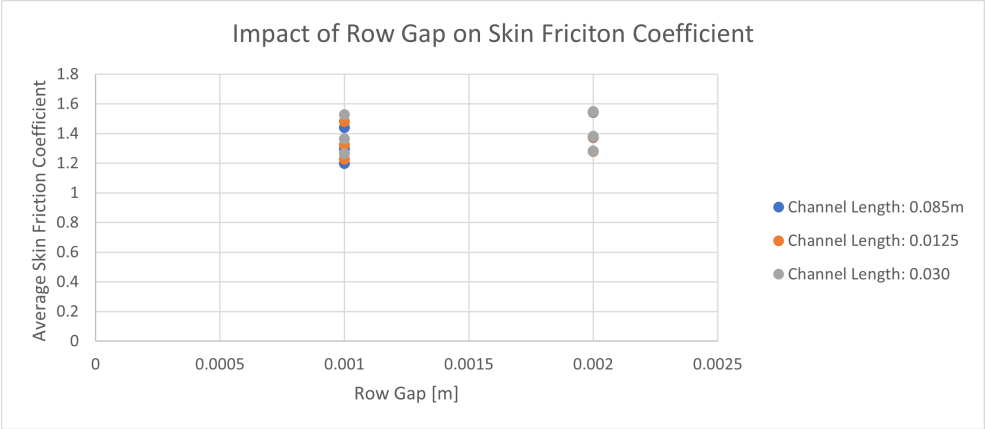

Figure 11: Graph of the row gap and channel lengths effect on the skin friction coefficient

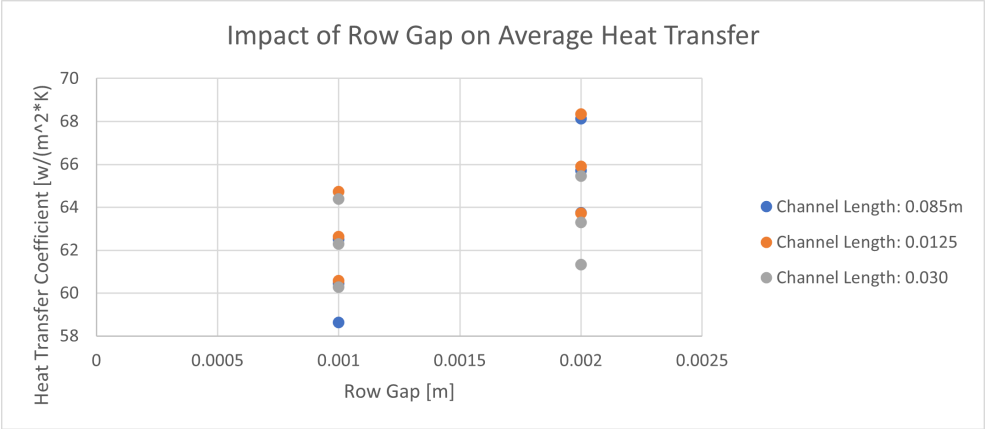

Figure 12: Graph of the row gap and channel lengths effect on the heat transfer coefficient

The figures below show images of the hydraulic boundary layers between two different row gaps.

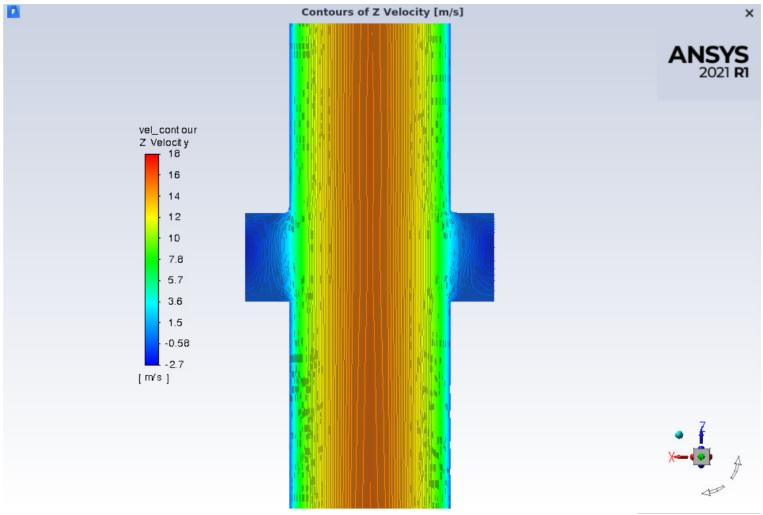

Figure 13: Temperature contour of a parallel geometry with fin gap ratio of 1.8, row gap of 2mm, and channel length of 0.0085

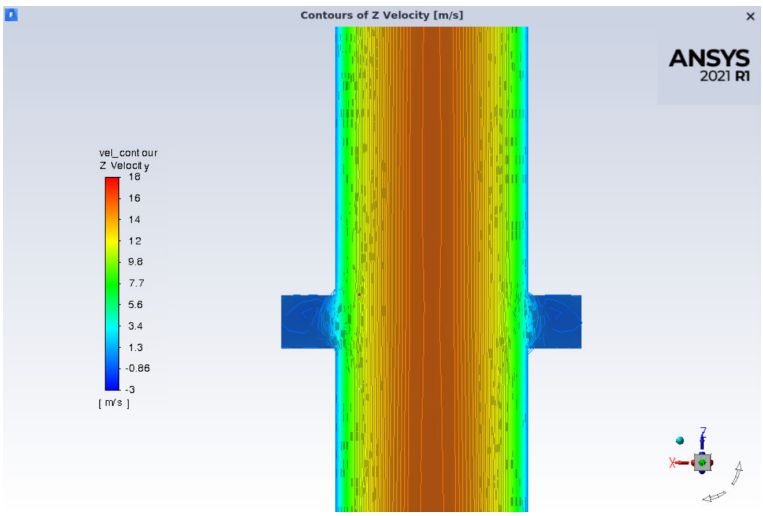

Figure 14: Temperature contour of a parallel geometry with fin gap ratio of 1.8, row gap of 1mm, and channel length of 0.0085

4.2.2 Offset Fin Results

The three graphs below in fig. 15, 16, and 17 show a comparison of the channel length and fin offset's impact on the skin friction coefficient, heat transfer coefficient, and the FOM.

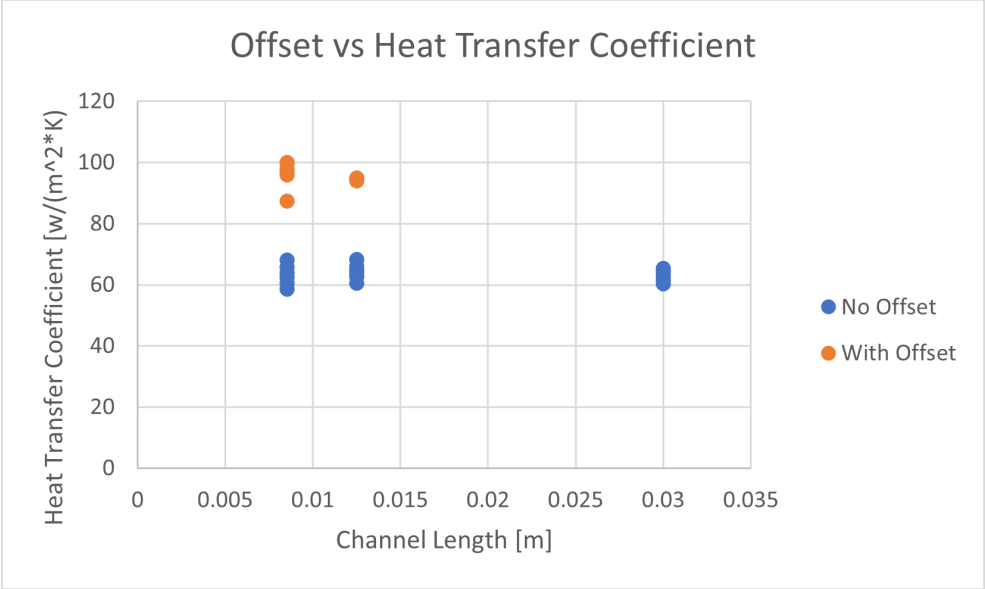

Figure 15: Graph of Fin Offset,Channel Length, and Heat Transfer Coefficient

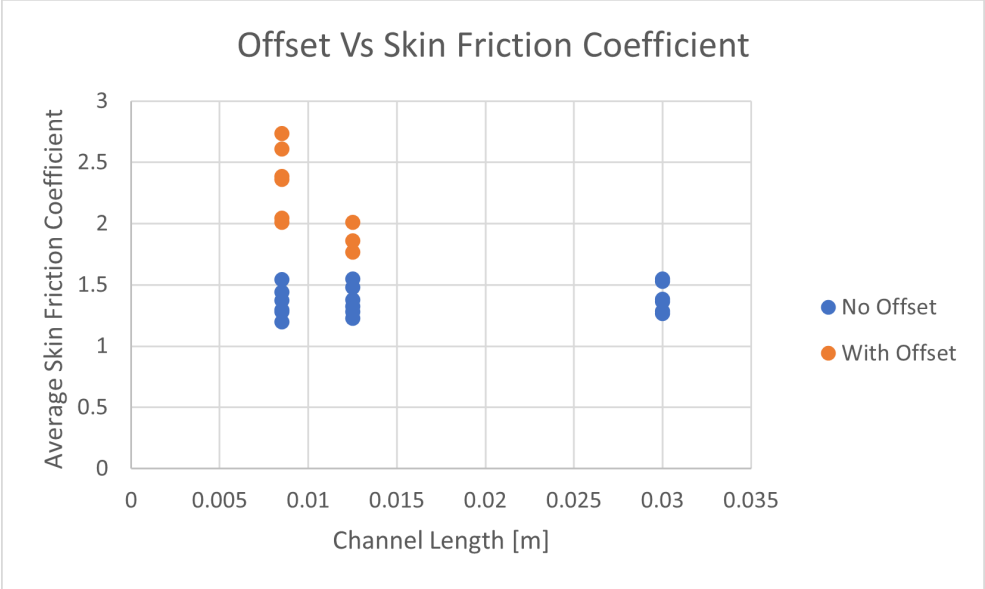

Figure 16: Graph of Fin Offset,Channel Length, and Skin Friction Coefficient

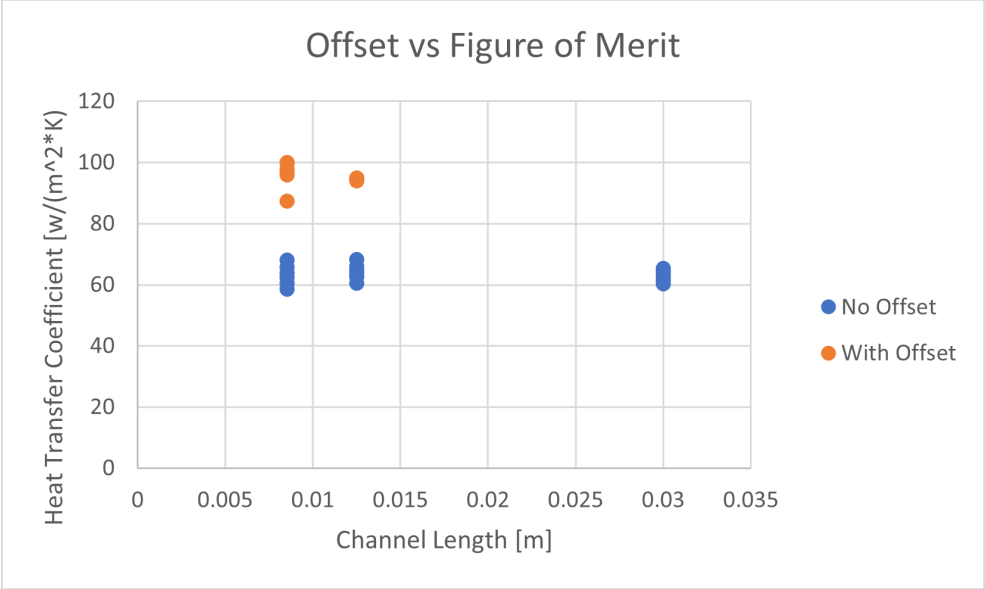

Figure 17: Graph of Fin Offset,Channel Length, and FOM

The two images below show images of the temperature and velocity profiles of the airflow around the offset fin heatsink.

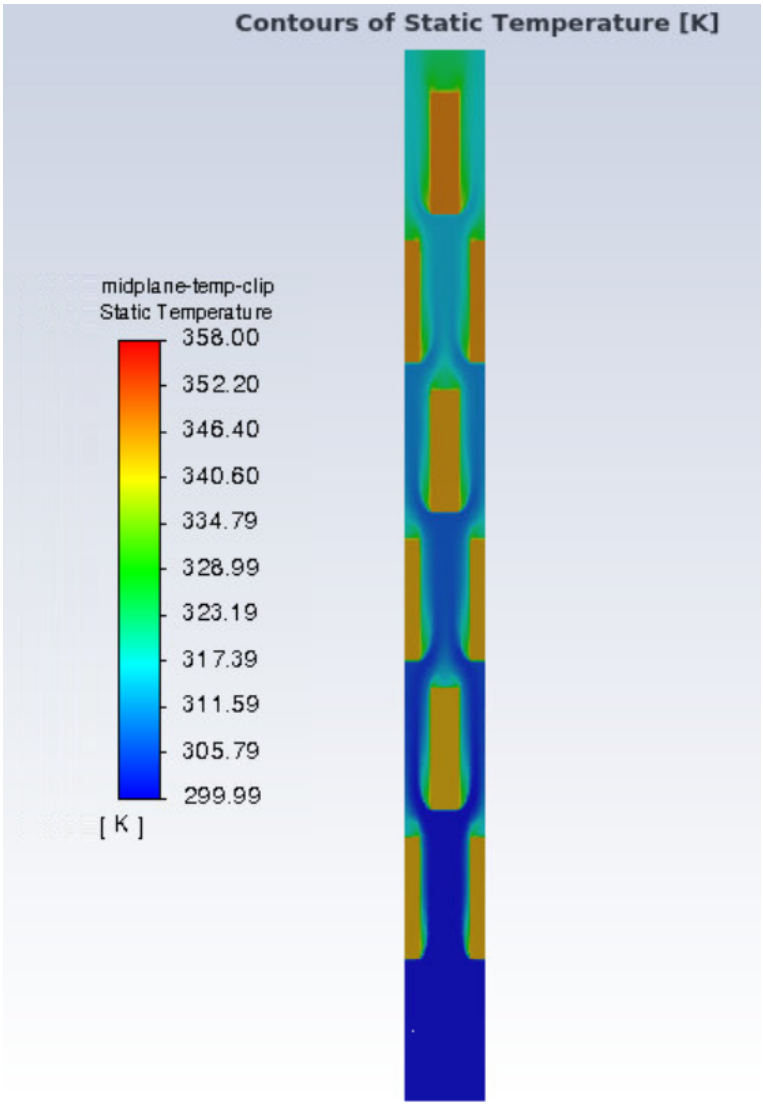

Figure 18: Temperature Contour for an offset geometry, fin gap ratio 1.8, channel length of 0.0085m, and row gap of 2mm

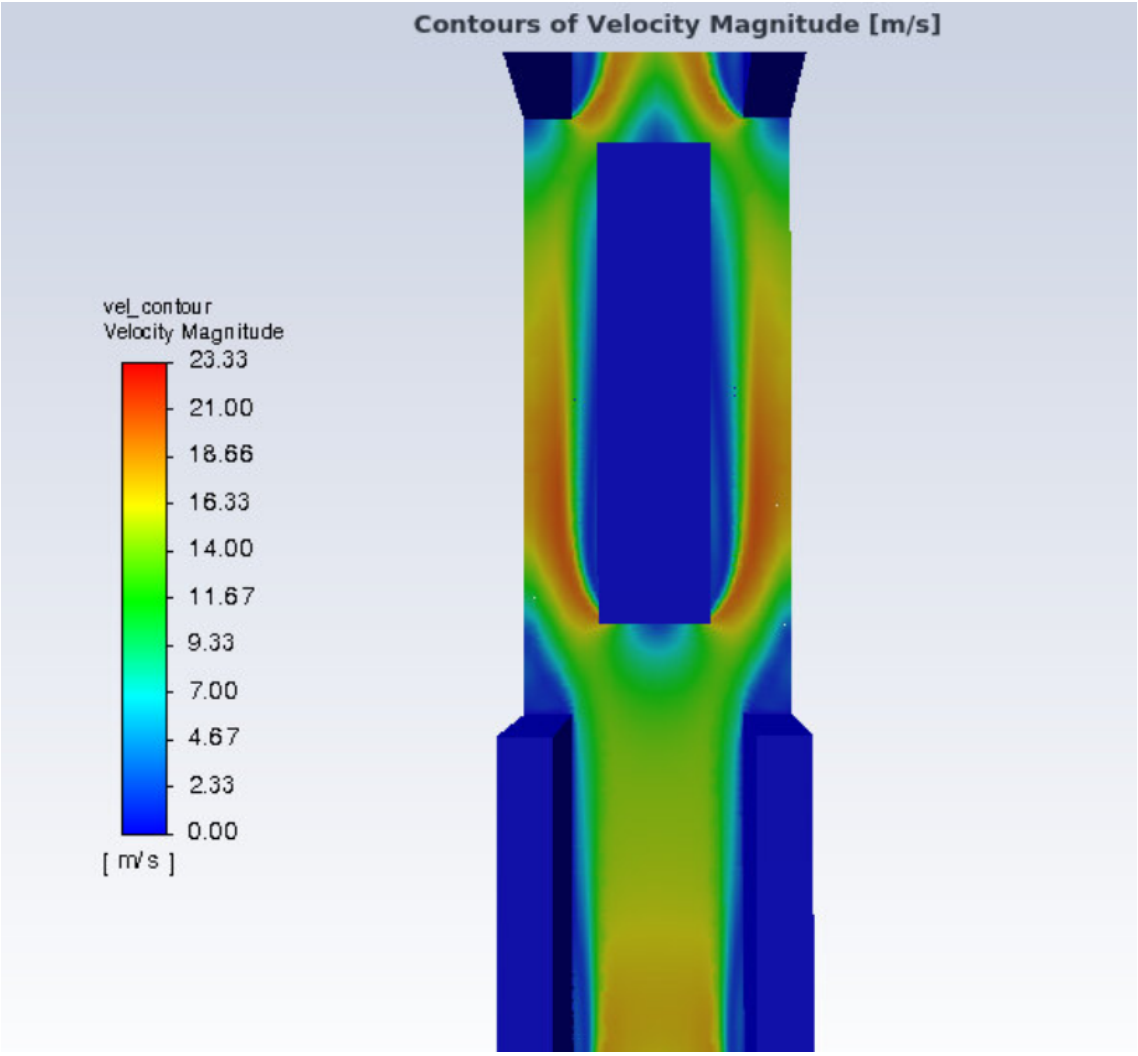

Figure 19: Velocity Contour for an offset geometry, fin gap ratio 1.8, channel length of 0.0085m, and row gap of 2mm

Lastly, the table below in fig. 20 shows the full data output of the simulation suite for both the inline and offset heatsinks.

Trial Number	Fin Gap Ratio	Row Gap [m]	Fin Offset	Average Skin Coefficient	Average Heat Transfer Coefficient [W/(m^2*K)]	Nusselt Number	FOM
0	1.5	0.002	0	1.5482	65.451	4.658434	1
1	2	0.002	0	1.2828813	61.321	4.364484	0.99747
2	1.8	0.002	0	1.3812	63.292	4.504769	1.00452
3	1.5	0.001	0	1.5295	64.387	4.582705	0.987724
4	2	0.001	0	1.2648643	60.291	4.291174	0.985374
5	1.8	0.001	0	1.3637	62.300039	4.434166	0.992975
6	1.5	0.002	0	1.5456	68.337	4.863843	1.044658
7	2	0.002	0	1.2792	63.721	4.535302	1.037474
8	1.8	0.002	0	1.3769	65.899553	4.69036	1.046972
9	1.5	0.001	0	1.4817	64.74	4.607829	1.003711
10	2	0.001	0	1.2264	60.573	4.311246	1.000205
11	1.8	0.001	0	1.3225	62.627	4.457438	1.008451
12	1.5	0.002	0	1.5424	68.12	4.848399	1.042085
13	2	0.002	0	1.2811	63.743	4.536868	1.037354
14	1.8	0.002	0	1.3725	65.706	4.676584	1.045011
15	1.5	0.001	0	1.441	62.512	4.449253	0.978196
16	2	0.001	0	1.1983	58.634	4.173238	0.975707
17	1.8	0.001	0	1.2965	60.453	4.302705	0.979882
18	1.5	0.002	0.5	2.3607	96.012	6.833594	1.274478
19	2	0.002	0.5	2.0126	87.355	6.217438	1.222902
20	1.8	0.002	0.5	2.044	97.756	6.957722	1.347547
21	1.5	0.001	0.5	2.7373	96.96	6.901068	1.225111
22	2	0.001	0.5	2.3833	99.822	7.104769	1.320871
23	1.8	0.001	0.5	2.6089	99.991	7.116797	1.28382
24	1.5	0.002	0.5	2.0109	95.007	6.762064	1.3304
25	2	0.002	0.5	1.7684	93.912	6.684128	1.372638
26	1.8	0.002	0.5	1.8588	94.688	6.739359	1.361148

Figure 20: Table of the Design Parameters and Simulation Results

5 Discussion and Conclusion

5.1 Comparison of Analytic and Numerical Models

When comparing the analytic and numeric solutions, the analytical solution predicted an average heat transfer coefficient of 105.12 $\frac{W}{m^2K}$, while the numerical solution for the same configuration predicted an average heat transfer coefficient of 65.9 $\frac{W}{m^2K}$. The predominant reason for the discrepancy between the analytical and numerical solutions for the flow between parallel plates comes down the the fin lengths. For the lengths under study, the Channel Reynolds numbers is 522.72, and the analytical model was only accurate for channel Reynolds numbers between 0.26 and 175. The solution accuracy would begin to decrease as the Channel Reynolds number increases.Additionally, the analytical model assumes that the flow begins to fully develop when entering the second row of fins, which would over predict the average Nusselt number. Another difference between the analytical and numerical model, is that the analytical model does not account for the change in bulk fluid temperature between the first and second row of fins. This could be mitigated in future work by determining the heat transfer from the first row of fins, and then calculating the change in average fluid temperature, and then using that value when calculating the heat transfer from the second row of fins instead of the original free stream fluid

temperature. This could be modified into an iterative model and used to calculate the heat transfer over an arbitrary number of rows.

5.2 Numerical Methods

For the parallel fin geometries, Figure 11 and 12 demonstrates that a larger row gap leads to increased heat transfer coefficients without an increase in skin friction coefficient. The key takeaway from fig. 11 is that other factors such as the channel length have a greater impact on the average skin friction coefficient. Upon further analysis of the CFD data, fig. 14 demonstrates that a smaller row gap does not significantly disrupt the hydraulic or thermal boundary layer boundary layer. When comparing the disruption in the boundary layer between a 1mm and 2mm row gap

The main conclusions that can be drawn from all of the simulation results is that the larger row gap leads to increases in heat transfer of 8% , while the offset leads to an increase in heat transfer by 39.5%. The increase in row gap increases the FOM by 6.5%, while the offset leads to increases of the FOM by 30.3%. This demonstrates that the addition of the offset is the driving increase in both heat transfer and the FOM. For the offset geometries, the main reason for the significant increase in heat transfer comes from the increase in velocity around the offset fin, as well as the large areas of detachment around each fin. These zones lead to a significant amount of mixing, which increases the heat transfer coefficient. By shifting the rows of fins over, the flow is forced to reenter the channel between the fins, which results in higher Nusselt number than the co-linear rows of fins.

5.3 Future Work

Unfortunately, a full design of experiments was not able to be conducted, so future work should seek to complete the DOE and create interaction plots to understand the interactions of all of the design variables. Additionally, a Reduced Order Model (ROM) should be developed in order to more rapidly design future heatsinks. The design space could also be expanded to consider an offset of 0.25, which would serve as a middle point between an no offset (offset=0) and having the rows completely offset (offset=0.5).With the full factorial DOE and ROM, recommendations towards the optimal combination of row gap, fin gap ratio, and channel length could be made. Additionally, a more detailed transient Large Eddy Simulation could be used to understand the structure of the turbulence generated by the offset. The CFD models should also be validated with a physical experiment on both the inline and offset fins. Lastly, more work should be done to look into the implementation of offset skived heatsinks in thermal management solutions. Skived heatsinks are commonly used in cold plates, with water as the heat transfer fluid, so an investigation into the impact of different hydraulic and thermal properties of the water should be conducted.

References

[1] A. Dutton, A. Levy, and D. Luberda, "Modification of skiving blades to create offset-fin heat sink," 2021, mcKelvey School of Engineering, Washington University in St. Louis.

[2] D. Luberda, "A modification to the skiving process for the manufacture of offset geometry strip-fin heat sinks," 2022, mcKelvey School of Engineering, Washington University in St. Louis.

[3] T. L. Bergman, *Fundamentals of heat and mass transfer*, 7th ed. J. Wiley amp; Sons, 2011.

[4] B. R. Munson, *Fundamentals of Fluid Mechanics*, 7th ed. Wiley, 2013.

[5] P. Teertstra, M. Yovanovich, J. Culham, and T. Lemczyk, "Analytical forced convection modeling of plate fin heat sinks," in *Fifteenth Annual IEEE Semiconductor Thermal Measurement and Management Symposium (Cat. No.99CH36306)*, 1999, pp. 34–41.

[6] F. M. White and J. Majdalani, *Viscous Fluid Flow*, 4th ed. McGraw-Hill, 2022.

[7] "Ansys fluent, 2022 r2, help system, fluent theory guide, [4.4.3]."

[8] "Ansys fluent, 2022 r2, help system,fluent theory guide, [4.1.1]."

[9] "Ansys fluent, 2022 r2, help system,fluent theory guide, [5.2.1]."

[10] Z. Huang, G. Yu, Z. Li, and W. Tao, "Numerical study on heat transfer enhancement in a receiver tube of parabolic trough solar collector with dimples, protrusions and helical fins," *Energy Procedia*, vol. 69, pp. 1306–1316, 2015, international Conference on Concentrating Solar Power and Chemical Energy Systems, SolarPACES 2014. [Online]. Available: https://www.sciencedirect.com/science/article/pii/S1876610215004555

Appendix A

Table of Contents


```
clear all
close all
clc
addpath Functions
```

Geometry

```
fin_height=0.0254; %m
fin_length= 0.0125; %m
fin_thickness=0.002; %m
fin_gap_ratio=1.8;
fin_gap=fin_thickness*fin_gap_ratio;
num_fins=8;
heatsink_width= (fin_thickness+fin_gap)*num_fins;
heat_transfer_area=2*fin_length*fin_height*num_fins;
```

Model Inputs

```
T_air=25;% deg Cfin g
T_base=85;% deg C
U= 10; % m/s
film_temp=(T_air+T_base)/2;
```

Material Properties

taken from Fundamentals of Heat and Mass Transfer 7th edition

```
k_heatsink=177; %2024-t6
Pr=AirProperties(film_temp,[],[],'Pr');
rho=AirProperties(film_temp,[],[],'rho');
k_air=AirProperties(film_temp,[],[],'k');
mu=AirProperties(film_temp,[],[],'mu');
```

```
nu=mu/rho;
```

Developing Flow Calculations

```
% Since we are introducing a break in the fins to disrupt the formation of
% the thermal boundary layer, we need to calculate the length of the
% development region within the fin

%first calculate the hydraulic diameter of the rectangle between the fins
%based on the fin geometry
area= fin_height*fin_gap;
perimeter=2*(fin_height+fin_gap);
D_h=4*area/perimeter;
Re_dh=U*D_h/mu; % Reynolds number based off of the hydraulic diameter

%determine the graetz number for a range of inlet lengths based off of the
%hydraulic diameter and the Reynolds number from the hydraulic diameter
critical_graetz=0.05; % this is the graetz number when the flow transitions
 from developing to developed
x_crit=critical_graetz*Re_dh*Pr*D_h;
x=linspace(0.001,2*x_crit,10000);
GZ_h=D_h./x*Re_dh*Pr;

Nu_developing=((3.66./(tanh(2.264.*GZ_h.^(-1/3)+1.7.*GZ_h.^(-2/3))))+...
    0.0449.*GZ_h.*tanh(GZ_h.^-1))./(tanh(2.432*Pr^(1/6).*GZ_h.^(-1/6)));
plot(x,Nu_developing,"LineWidth", 1)
xline(x_crit)
title('Nusselt Number in the Entrance region between fins')
subtitle('Fin height: 0.0254m, Fin gap:0.0036 m')
xlabel('Position along the fin in the streamwise direction [m]')
ylabel('Nusslt Number')
legend('Nusselt Number')
```

Y+ calculations

```
C_f=16/Re_dh;
wall_shear=0.5*C_f*rho*U^2;
U_t=sqrt(wall_shear/rho); % friction velocity
yplus=1;
y=yplus*nu/U_t; %distance from the wall to achieve a yplus of 1 in m
```

1D Analytical model

Analytical Forced Convection Modeling of Plate Fin Heat Sinks

```
n=3; %blending factor between developing and developed nusslt numbers
```

Dimensionless Constants

```
Re_b=U*fin_gap/mu; %Reynolds number from analytical modeling paper
Re_b_star=Re_b*fin_gap/fin_length;
```

```
%Not using the developed nusslt number since the flow never fully develops
% Nu_fd=0.5*Re_b_star*Pr; % Fully Developed Flow nusslt Number
Nu_dev=0.664*sqrt(Re_b_star)*Pr^(1/3)*(1+(3.65/sqrt(Re_b_star)));
% Nusslt Number for developing flow between two plates
% Nu_blend=((1/Nu_fd)^n+(1/Nu_dev)^n)^(-1/n); % blending between the two
 nusslt numbers
%power mean????

Nu_blend=Nu_dev;
```

Fin Effects

```
P=2*fin_thickness+2*fin_length;
fin_area=fin_thickness*fin_length;
h=Nu_blend*k_air/fin_gap;
m=sqrt(h*P/(k_heatsink*fin_area));
eta=tanh(m*fin_height)/(m*fin_height);
Nu_fin_effect=eta*Nu_blend;

final_heat_transfer_coef=Nu_fin_effect*k_air/fin_gap;
```

Solution

```
fin_heat_transfer=Nu_fin_effect*k_air*(fin_length*fin_height)*(T_base-T_air)/
fin_gap;
total_heat_transfer=num_fins*fin_heat_transfer;
total_fin_area=fin_area*num_fins;
```

Published with MATLAB® R2022a